Dalton Transactions

ROYAL SOCIETY OF CHEMISTRY

PAPER

View Article Online
View Journal | View Issue

Cite this: *Dalton Trans.*, 2023, **52**, 8670

Hierarchical subcomponent self-assembly of covalent triple-stranded complexes with 3d–4f vertices: luminescence and magnetic properties†

Zhi Liu,[a,b] Fan Yin,[a,b] Jian Yang,[b] Xiao-Qing Guo,[b] Li-Peng Zhou,[b] Chong-Bin Tian *[a,b] and Qing-Fu Sun *[a,b]

Received 15th April 2023,
Accepted 19th May 2023

DOI: 10.1039/d3dt01139a

rsc.li/dalton

Well-defined 3d–4f heterometallic supramolecular architectures have attracted attention because of their applications in the field of luminescence and magnetism. However, covalent metallo-supramolecular discrete complexes, decorated with hetero-metallic vertices, have never been reported because of the difficulties in design and control. Herein, we report a series of covalent metallo-supramolecular discrete complexes with 3d–4f vertices synthesized by hierarchical subcomponent self-assembly of tris(2-aminoethyl)amine, 2,6-diformyl-*p*-cresol, and lanthanide ions (Ln) with different amines and transition metal ions. The programmable self-assembly process results in the formation of triple-stranded hetero-metallic covalent organic discrete complexes, namely **3a–3c-(Ln, Zn)** (Ln = Sm^{III}, Eu^{III}, Dy^{III}, Yb^{III} and Lu^{III}) and **3a′-(Dy, Co)**, which are characterized by nuclear magnetic resonance (NMR) analysis, electrospray ionization time-of-flight mass spectrometry (ESI-TOF-MS), and single-crystal X-ray analysis. Photophysical investigations disclose that the organic skeleton of **3a-(Ln, Zn)** exhibits an excellent sensitizing ability toward Sm^{III}, Eu^{III}, and Yb^{III} ions, displaying characteristic luminescence emission in both the visible and near-infrared (NIR) regions. AC susceptibility measurements of **3a′-(Dy, Co)** reveal the frequency-independent performance under zero dc field, suggesting the absence of slow relaxation of magnetization. This work offers a new approach for the fabrication of discrete metallic covalent architectures with 3d–4f vertices.

Introduction

Over the past few decades, coordination-driven self-assembly, as a powerful synthesis technique, has been employed by many chemists in the construction of various supramolecular architectures.[1–7] By referring to the template synthesis of Busch,[8] Nitschke extended the synthesis technique and proposed the versatile "subcomponent self-assembly" strategy.[9] In this strategy, the metal–ligand coordination bonds and covalent dynamic imine bonds (formed by condensation of an amine and an aldehyde) are *in situ* formed.

A myriad of diverse metallo-supramolecular compounds with sophisticated structures and fascinating functions, including, but not limited to, macrocycles,[10–12] helicates,[13–15] grids,[16,17] catenanes,[18] rotaxanes,[19] and metal–organic polyhedra,[20–23] have been successfully fabricated by the subcomponent self-assembly approach. Besides these types of structures, there is another type of structure composed of a discrete covalent organic skeleton and metal ions, namely discrete covalent metallo-supramolecular architectures, in which the metal ions are located at the vertices or panels of the covalent organic skeleton. This type of structure is particularly appealing, since the introduction of metal ions not only can template the synthesis of covalent organic cages or covalent organic macrocycles[24–26] that cannot be acquired by traditional direct imine condensation,[27–32] but also endow the structure embedded by metal ions with special functions.[22,23,33–35] Therefore, templated metal ions play a dominant role in determining the structures and functions of discrete covalent metallo-supramolecular complexes. If two different metal ions, such as transition metal ions (3d) and lanthanide ions (4f), are simultaneously introduced into such systems, the intrinsic optical and large single-ion magnetic anisotropy of lanthanides together with remarkable magnetic interactions between 3d and 4f make such 3d–4f based complexes excellent candidates for luminescent materials and single molecular magnets (SMMs).[36–40] As far as we are aware, however, the syntheses of covalent metallo-supramolecular complexes were primarily based

[a]*College of Chemistry, Fuzhou University, Fuzhou 350108, People's Republic of China. E-mail: tianchongbin@fjirsm.ac.cn, qfsun@fjirsm.ac.cn*
[b]*Fujian College, University of Chinese Academy of Sciences, Fuzhou 350002, People's Republic of China*

† Electronic supplementary information (ESI) available. CCDC 2256435–2256438. For ESI and crystallographic data in CIF or other electronic format see DOI: https://doi.org/10.1039/d3dt01139a

on single transition metal ions,[25,26,30,41–48] very limited to single lanthanide ions.[35] In contrast, 3d-4f heterometallic ions have not been explored, largely because of the challenge of designing a suitable ligand that can bridge the gap between the divergent coordination preferences and abilities of 4f and 3d ions.

Previously, we reported several hetero-metallic cages or macrocycles by hierarchical self-assembly of Pd^{II} or Pt^{II} metallo-ligands with lanthanide ions.[49–53] With our continuing interest in hierarchical self-assembly, herein, we report the hierarchical subcomponent self-assembly of hetero-metallic covalent organic triple-stranded complexes. The subcomponent self-assembly of tris(2-aminoethyl)amine (TREN) and 2,6-diformyl-*p*-cresol (DFMP) with lanthanide ions (Ln) leads to the formation of metallo-ligand **1-Ln** (Scheme 1). The subsequent subcomponent self-assembly of preformed **1-Ln**, diamine (**2a** and **2b**), or triamine (**2c**) with transition metal ions gives rise to a family of heterometallic covalent organic triple-stranded molecules, that is **3a–3c-(Ln, Zn)** and **3a′-(Dy, Co)**, in which the hetero-metal nodes are situated at the vertices of triple-stranded molecules. Photophysical investigations indicate that the organic backbone of **3a-(Ln, Zn)** can not only sensitize the visible lanthanide ions (Ln = Sm^{III} and Eu^{III}), but also sensitize NIR-region Yb^{III} ions. Moreover, the magnetic properties of **3a′-(Dy, Co)** are also studied.

Experimental section

Synthesis of subcomponent 1-Ln

Metallo-ligands **1-Dy**, **1-Lu** and **1-Yb** were synthesized according to previously reported literature.[54] By substitution of Ln $(OTf)_3{\cdot}9H_2O$ with $Ln(NO_3)_3{\cdot}6H_2O$, the metallo-ligands **1-Sm** and **1-Eu** were also prepared with yields of 35% and 30%. **1-Sm**: ^{1}H NMR (400 MHz, DMSO-d_6) δ 10.53 (s, 1H), 7.56 (d, J = 2.2 Hz, 1H), 7.43 (s, 1H), 7.40 (d, J = 2.2 Hz, 1H), 3.73 (s, 2H), 2.63 (s, 2H), 2.23 (s, 3H). ESI-TOF-MS for **1-Sm**: calcd for [(**1-Sm**) + Na]$^+$ 756.1431, found 756.1488; [(**1-Sm**)$_2$ + Na]$^+$ 1486.3057, found 1486.3075. ESI-TOF-MS for **1-Eu**: calcd for [(**1-Eu**) + Na]$^+$ 757.1508, found 757.1496.

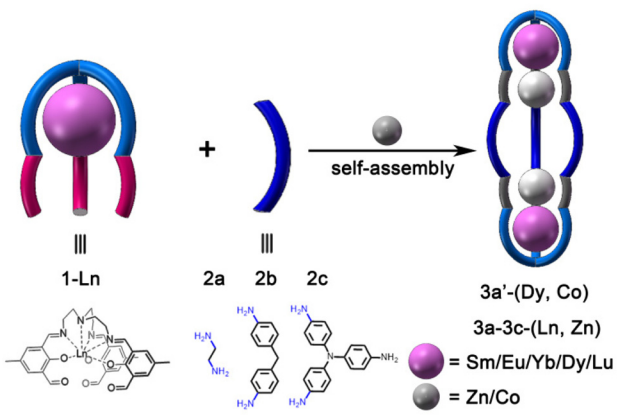

Scheme 1 Self-assembly of **3a–3c-(Ln, Zn)** and **3a′-(Dy, Co)**.

Synthesis of complex 3a-(Sm, Zn)

Metallo-ligand **1-Sm** (7.32 mg, 0.01 mmol) was mixed with ethylenediamine (0.9 mg, 0.15 mmol) in a mixture of 1 : 1 chloroform and methanol. After heating at 50 °C for about 5 h, the suspension was centrifuged to obtain a precipitate. When the precipitate was dissolved in 600 μL of acetonitrile-d_3 in the presence of 1.0 eq. $Zn(OTf)_2$, a homogeneous yellow solution was obtained. ^{1}H NMR (400 MHz, Acetonitrile-d_3) δ 8.91 (s, 1H), 7.64 (d, J = 1.7 Hz, 1H), 7.30 (d, J = 1.7 Hz, 1H), 6.94 (s, 1H), 4.71–4.50 (m, 2H), 4.39–4.16 (m, 3H), 3.76–3.65 (m, 1H), 2.30 (s, 3H). ESI-TOF-MS for **3a-(Sm, Zn)**: the following picked signals are those at the highest intensities. m/z calcd for **[3a-(Sm, Zn)(OTf)$_2$]$^{2+}$** 983.1101, found 983.1085; calcd for **[3a-(Sm, Zn)(OTf)$_1$]$^{3+}$** 605.7559, found 605.7555.

The synthesis procedures of **3a′-(Dy, Co)**, **3b-(Ln, Zn)** and **3c-(Ln, Zn)** were similar to that of **3a-(Sm, Zn)** by changing the amine or metal source (see the ESI† for details).

Results and discussion

As shown in Scheme 1, **3a′-(Dy, Co)** and **3a–3c-(Ln, Zn)** (Ln = Sm^{III}, Eu^{III}, Dy^{III}, Yb^{III} and Lu^{III}) were synthesized through subcomponent self-assembly of **1-Ln** with different amines in the presence of transition metal ions. As a representative example, the subcomponent self-assembly of **3a-(Sm, Zn)** was investigated. The ^{1}H NMR spectrum reveals the generation of a sole species with a high degree of symmetry other than oligomeric species (Fig. 1B). Compared with metallo-ligand **1-Sm**, all singles stemming from the formed species are shifted, in agreement with the coordination to Zn^{2+} ions. Moreover, ^{1}H diffusion ordered spectroscopy (DOSY) displays that all signals are located at the same diffusion band (Fig. 1C), further confirming the single species in solution. Using the Stokes–Einstein equation, the diffusion coefficients and dynamic radius were estimated to be 1.0×10^{-9} m^2 s^{-1} and 6.33 Å, respectively. As displayed in Fig. 1D, electrospray ionization time-of-flight mass spectroscopy (ESI-TOF-MS) again suggests the formation of the expected hetero-metallic covalent organic triple-stranded molecule with the formula of **3a-(Sm, Zn)·(OTf)$_4$**. Two main peaks (m/z = 605.7555 and 982.1086) observed in the ESI-TOF-MS spectrum can be assigned to **[3a-(Sm, Zn)·OTf]$^{3+}$** and **[3a-(Sm, Zn)·(OTf)$_2$]$^{2+}$**, respectively. The assignments of these peaks are also confirmed by the careful comparison of the experimental data with the simulated isotopic distributions (Fig. 1D, inset). After changing **2a** with **2b** or **2c**, the ESI-TOF-MS confirms the formation of **3b-(Sm, Zn)** or **3c-(Sm, Zn)** (Fig. 1E and F).

The formations of other covalent organic triple-stranded molecules were also identified by various characterization methods including NMR (^{1}H, COSY, DOSY), ESI-TOF-MS and single-crystal X-ray diffraction studies, which are highly consistent with the expected stoichiometry.

Attempts to solve the crystal structures of **3a–3c-(Sm, Zn)** failed, as we cannot get single crystals of **3a–3c-(Sm, Zn)**. However, upon replacing Sm^{III} with Lu^{III}, the single crystals of

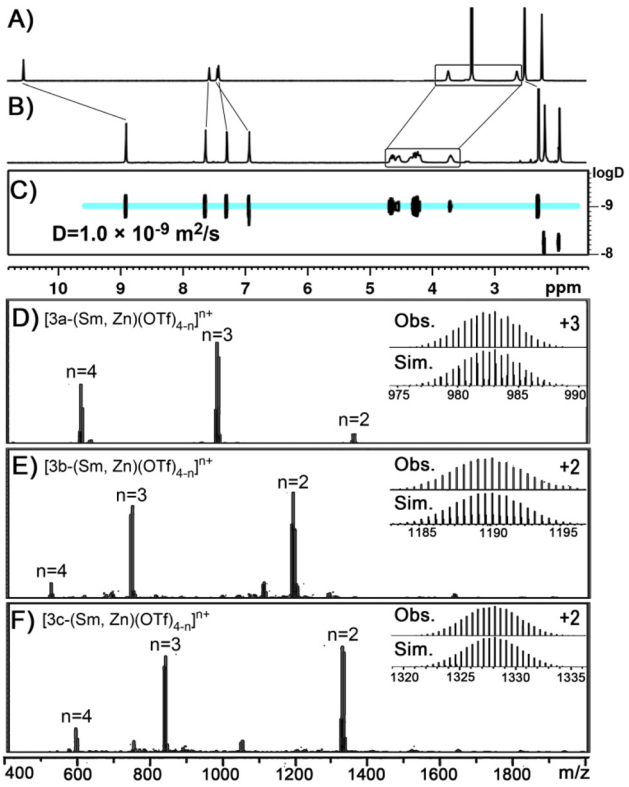

Fig. 1 ^{1}H NMR (400 MHz, 298 K) spectra of **1-Sm** in DMSO-d_6 solution (A) and **3a-(Sm, Zn)** in CD_3CN solution (B). ^{1}H DOSY NMR (400 MHz, 298 K, CD_3CN) spectrum of complex **3a-(Sm, Zn)** (C). ESI-TOF-MS spectra of (D) **3a-(Sm, Zn)**, (E) **3b-(Sm, Zn)** and (F) **3c-(Sm, Zn)**.

3a–3c-(Lu, Zn), which were the isostructural compounds of **3a–3c-(Sm, Zn)**, were successfully obtained by slow vapor diffusion of ether (diethyl ether for **3a-(Lu, Zn)**, isopropyl ether for **3b-(Lu, Zn)** and methyl tertiary-butyl ether for **3c-(Lu, Zn)**) into the acetonitrile solutions of the corresponding assemblies. Single-crystal X-ray diffraction analysis shows that **3a–3c-(Lu, Zn)** are the hetero-metallic triple-stranded covalent organic molecules, where hetero-metallic Lu–Zn nodes are located at the vertices of the molecules (Fig. 2). The refinement

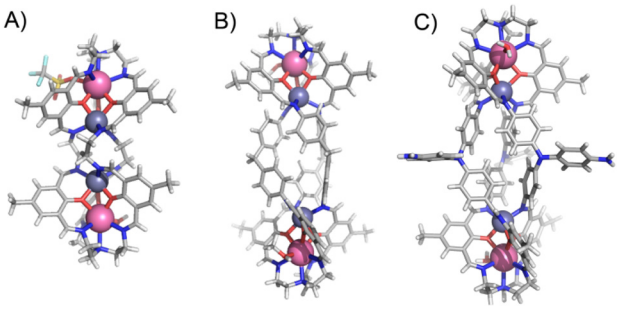

Fig. 2 X-Ray crystal structures of (A) **3a-(Lu, Zn)**, (B) **3b-(Lu, Zn)** and (C) **3c-(Lu, Zn)** where the free counter-ions and solvent molecules are omitted for clarity. (C, gray; H, white; N, blue; O, red; Lu, magenta; Zn, dark gray; S, yellow; F, cyan).

parameters and crystallographic data for **3a–3c-(Lu, Zn)** are shown in Tables S1 and S2.† The important bond distances (Å) and angles (°) for **3a–3c-(Lu, Zn)** are listed in Tables S3–S5.† Both **3a-(Lu, Zn)** and **3b-(Lu, Zn)** crystallized in the monoclinic $C2/c$ space group, while **3c-(Lu–Zn)** crystallized in the $P\bar{1}$ space group. To the best of our knowledge, these complexes represent the first example of covalent organic metallo-supramolecular molecules with 3d–4f hetero-metallic vertices.

Considering the very similar structure of **3a–3c-(Lu, Zn)**, only the structural description of **3a-(Lu, Zn)** will be given here in detail. As shown in Fig. 2A, the **3a-(Lu, Zn)** molecule consists of two Lu^{III} ions, two Zn^{III} ions, one triple-stranded covalent organic backbone, one coordinated OTf^- anion and one coordinated H_2O molecule. The three strands of the covalent organic backbone wrap around the four metal centers (two Lu^{III} and two Zn^{III} ions) and form the heterometallic covalent organic triple-stranded assembly. Both the Lu1 and Lu2 atoms are eight-coordinated, adopting a triangular dodecahedron (TDD-8) coordination geometry (Table S9†) with different coordination environments: the Lu1 atom is ligated by four nitrogen atoms (N1, N2, N3 and N4) from the TREN unit, three oxygen atoms (O2, O3 and O4) from the phenolic groups of the covalent organic backbone and one oxygen atom (O1) from the coordinated water molecule, while the Lu2 atom is surrounded by four nitrogen atoms (N11, N12, N13 and N14) from the TREN unit, three oxygen atoms (O5, O6 and O7) from the phenol groups and one oxygen atom (O8) from the coordinated OTf^- anion (Fig. S58†). The bond distance of Dy–O_{phenol} is shorter than the others, owing to the strong coordination ability of the deprotonated phenolic oxygen atoms toward the Lu atoms. The bond length between the lanthanide center and the tertiary amine N atom of TREN (Lu–N1 or Lu–N11) is the longest among the Lu–O/N bond lengths, which can be ascribed to the limitation of the conformation of TREN. Unlike the Lu atoms, two Zn atoms are six-coordinated and coordinated by three nitrogen atoms from the three covalent C=N groups and three oxygen atoms from three phenol groups belonging to the three strands of the covalent organic backbone, forming a OC-6 coordination geometry (Table S10†). The phenolic oxygen atoms in the covalent organic backbone adopt the μ_2-OR coordination model, *i.e.*, the Lu^{III} ion and Zn^{II} ion are connected together by phenolic oxygen and produce the hetero-metallic nodes, in which the average Lu–O–Zn bond angle is 94.28° and the average Lu–Zn distance is 3.23 Å. The distance between the tertiary amine N atoms of TREN (N1–N11) is 16.62 Å in **3a-(Lu, Zn)**, which is shorter than those in **3b-(Lu, Zn)** (23.03 Å) and **3c-(Lu, Zn)** (23.13 Å).

It should be noted that the covalent organic tetrahedron may be obtained if the tritopic triamine subcomponent was used, as observed in the previous reports.[35,42,44] However, in our work, only the discrete covalent organic triple-stranded compound was observed when the ditopic diamine subcomponent was replaced with the tritopic triamine subcomponent. In **3c-(Lu, Zn)**, the three coordination atoms closest to the panel backbone are three nitrogen atoms originating from three

imine bonds (C═N), while the corresponding atoms in the reported examples are three pyridine nitrogen atoms. This difference should be responsible for the formation of a triple-stranded compound other than the tetrahedron, due to the dihedral angle generated by the plane of three coordinated nitrogen atoms closest to the panel backbone and one benzene ring plane of the tritopic subcomponent in **3c-(Lu, Zn)** is about 98°, which is much smaller than the corresponding angle (≈120°) in the tetrahedron (Fig. S62†).

Photophysical properties

The UV-vis absorption and luminescence properties of **3a–3c-(Sm, Zn)** were measured in solution at room temperature. Upon excitation at 386 nm, the organic skeleton of **3a-(Sm, Zn)** can well sensitize Sm^{III}, while the organic backbone of **3c-(Sm, Zn)** cannot sensitize Sm^{III} (Fig. 3a). Five characteristic bands at 561, 609, 645, 705 and 787 nm can be clearly found for complex **3a-(Sm, Zn)**, corresponding to the transitions from the emitting $^4G_{5/2}$ to the ^6H_J (J = 5/2–13/2) states. To gain insight into the differences observed in the emission spectra, the phosphorescence spectra of complexes **3a–3c-(Gd, Zn)** were measured at 77 K (Fig. S54†), from which the triplet state energy levels of the organic skeletons were determined to be 21 053 cm^{-1}, 20 167 cm^{-1} and 17 605 cm^{-1} for **3a-(Gd, Zn)**, **3b-(Gd, Zn)** and **3c-(Gd, Zn)**, respectively. The organic skeleton triplet state energy level of **3c-(Gd, Zn)** is smaller than those of **3a-(Gd, Zn)** and **3b-(Gd, Zn)**, and can be comparable with the energy level of $^4G_{5/2}$ of Sm^{III} ions, meaning that the organic skeleton of **3c-(Gd, Zn)** cannot sensitize Sm^{III} ions. Thus, we infer that the difference in the organic skeleton triplet state energy level should be responsible for the distinct emission spectra of **3a–3c-(Sm, Zn)**.

Besides the Sm^{III} ion, the organic skeleton of **3a-(Sm, Zn)** can also sensitize other lanthanide ions, such as Eu^{III} ions and NIR-emissive Yb^{III} ions. As shown in Fig. 3b, complex **3a-(Eu, Zn)** exhibits apparent peaks at 592, 612, 650 and 700 nm, corresponding to the $^5D_0$ to ^7F_J (J = 0–4) transition of the Eu^{III} ion. For **3a-(Yb, Zn)**, it displays a well-resolved emission band at 977 nm, which can be assigned to the transition from the $^2F_{5/2}$ to the $^2F_{7/2}$ state. It is worth pointing out that the luminescence of the organic backbone (emission at about 456 nm, Fig. S41†) was not observed for complexes **3a-(Eu, Zn)** and **3a-(Yb, Zn)**, revealing the complete energy transfer from the organic skeleton to the lanthanide ions. In contrast, **3a-(Sm, Zn)** has a significant amount of the residual ligand emitted at about 456 nm, suggesting the incomplete organic skeleton to lanthanide energy transfer.[34]

Magnetic properties

Given that Co^{II} and Dy^{III} ions are the large magnetic anisotropy ions, and that once the super-exchange ferromagnetic interaction occurs between Co^{II} and Dy^{III}, quantum tunneling of magnetization (QTM) can be mitigated,[55,56] we prepared compound **3a′-(Dy, Co)** and characterized it through single-crystal X-ray diffraction, ESI-TOF-MS, TG, PXRD and elemental analysis (see the ESI†). The *M*–*H* curves (2, 3 and 5 K) and AC magnetic susceptibility were measured to testify the possible single

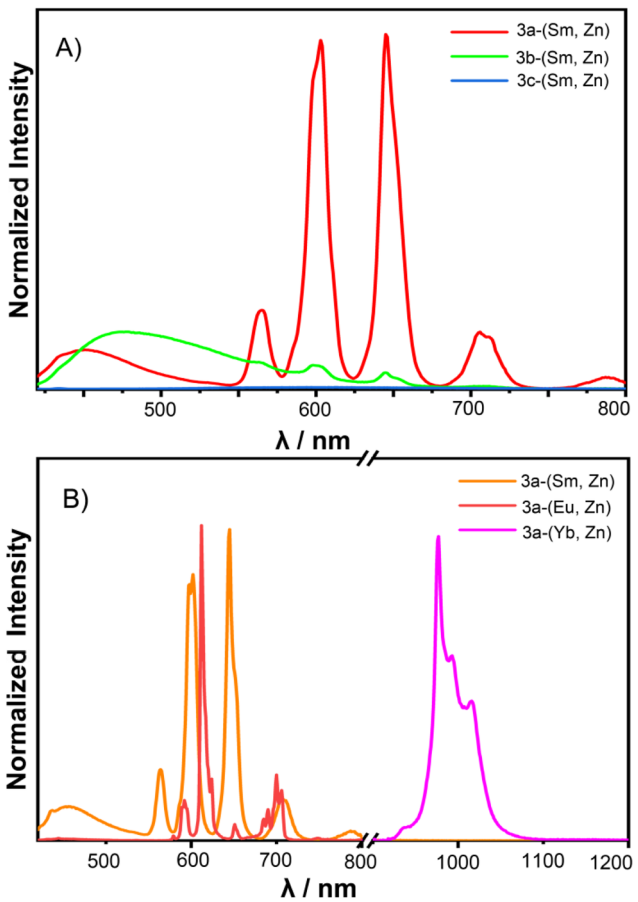

Fig. 3 (A) Emission spectrum of **3a–3c-(Sm, Zn)** (1.0 × 10^{-5} M in CH_3CN) at room temperature. (B) Emission spectrum of **3a-(Sm, Zn)**, **3a-(Eu, Zn)** and **3a-(Yb, Zn)** (1.0 × 10^{-5} M in CH_3CN) at room temperature.

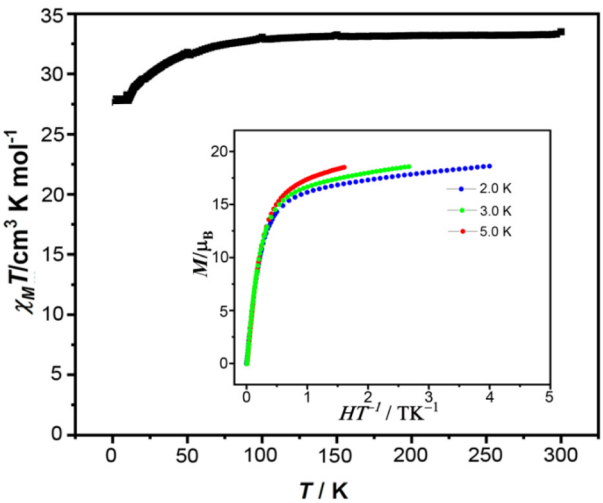

Fig. 4 Temperature-dependent $\chi_M T$ plots for **3a′-(Dy, Co)**. Insert: Field dependences of magnetization between 0 and 80 kOe and at temperatures of 2.0, 3.0, and 5.0 K.

molecular magnets properties of **3a′-(Dy, Co)**. As shown in Fig. 4, the observed $\chi_M T$ value at room temperature is 33.50 cm^3 K mol^{-1}, which is larger than the theoretical value of 32.09 cm^3 K mol^{-1} expected for two isolated Co^{II} ions (S = 3/2 and g = 2.0) and two isolated Dy^{III} ions (J = 15/2 and g = 4/3). Such a disparity should be attributed to the significant orbital contribution of the high-spin octahedral Co^{II} ions.[57–59] The $\chi_M T$ products remain nearly constant up to 100 K, below which they decrease slowly and reach the minimum value of 27.66 cm^3 K mol^{-1} at 2 K. The decreases below 100 K are likely to be caused by the depopulation of the Stark levels of Dy^{III} and the spin–orbital effect of Co^{II}. Moreover, the possible weak antiferromagnetic interactions between Dy^{III} and Co^{II} may also make some contributions to the decreases of $\chi_M T$ below 100 K, as observed in other heterometallic Co^{II}–Dy^{III} compounds.[60] The magnetization isotherm curves display a rapid increase at low fields and then a gradual increase at higher fields without reaching saturation even at 8 T, which is very common behavior for such compounds and indicative of the presence of anisotropy in this compound. As shown in Fig. S56,† no out-of-phase AC signals were found for **3a′-(Dy, Co)**, suggesting the absence of slow magnetization relaxation behaviour in **3a′-(Dy, Co)**. To further investigate the possible field-induced SMM behavior, field dependent x''_m data were collected to acquire an optimum dc field (Fig. S57†). From Fig. S57,† we can see that no maximum was found in the x''_m–H curve, indicating the absence of an optimum dc field. This phenomenon can be attributed to the relatively small energy barriers for the reverse of the magnetic moment in **3a′-(Dy, Co)**.[61]

Conclusions

In summary, a series of hetero-metallic covalent organic triple-stranded molecules with 3d–4f vertices have been synthesized through the hierarchical subcomponent self-assembly approach. These compounds are the first examples of covalent organic metallo-supramolecular backbones decorated with 3d–4f heteronuclear vertices. Besides, 3d–4f vertices of these complexes bring photophysical and magnetic properties to the assemblies. The luminescence investigations revealed that the organic backbone fabricated by using ethylenediamine can sensitize the luminescence emissions of lanthanide ions (Sm^{III}, Eu^{III} and Yb^{III}) in both the visible and NIR domains. The AC magnetic susceptibility measurements revealed the absence of slow magnetization relaxation behaviour in compound **3a′-(Dy, Co)**. This work confirms that the hierarchical subcomponent self-assembly is a potential route to fabricate discrete hetero-metallic covalent organic architectures.

Author contributions

The manuscript was written through the contributions of all authors. All authors have given approval to the final version of the manuscript.

Conflicts of interest

There are no conflicts to declare.

Acknowledgements

This work was funded by the National Natural Science Foundation of China (Grants 21971237, 21825107 and 22171264), the National Key Research and Development Program of China (Grant 2021YFA1500400), and the Science Foundation of Fujian Province (Grants 2021J02016 and 2022J01507).

References

1 X. Z. Li, C. B. Tian and Q. F. Sun, *Chem. Rev.*, 2022, **122**, 6374.
2 C. B. Tian and Q. F. Sun, *Chem. – Eur. J.*, 2023, **29**, e202300195.
3 R. Chakrabarty, P. S. Mukherjee and P. J. Stang, *Chem. Rev.*, 2011, **111**, 6810.
4 Y. Domoto and M. Fujita, *Coord. Chem. Rev.*, 2022, **466**, 214605.
5 M. Yoshizawa and L. Catti, *Acc. Chem. Res.*, 2019, **52**, 2392.
6 W. Liu, P. J. Das, H. M. Colquhoun and J. F. Stoddart, *CCS Chem.*, 2022, **4**, 755.
7 D. Chu, W. Gong, H. Jiang, X. Tang, Y. Cui and Y. Liu, *CCS Chem.*, 2021, **3**, 1692.
8 T. J. Hubin and D. H. Busch, *Coord. Chem. Rev.*, 2000, **200**, 5.
9 J. R. Nitschke, *Acc. Chem. Res.*, 2007, **40**, 103.
10 Q. Zhang, F. Chen, X. Shen, T. He, H. Qiu, S. Yin and P. J. Stang, *ACS Macro Lett.*, 2021, **10**, 873.
11 J. Dong, C. Tan, K. Zhang, Y. Liu, P. J. Low, J. Jiang and Y. Cui, *J. Am. Chem. Soc.*, 2017, **139**, 1554.
12 E. F. V. Dry, J. K. Clegg, B. Breiner, D. E. Whitaker, R. Stefak and J. R. Nitschke, *Chem. Commun.*, 2011, **47**, 6021.
13 J. Jiao, J. Dong, Y. Li and Y. Cui, *Angew. Chem.*, 2021, **133**, 16704.
14 J. R. Nitschke, D. Schultz, G. Bernardinelli and D. Gerard, *J. Am. Chem. Soc.*, 2004, **126**, 16538.
15 L. Wu, M. Tang, L. Jiang, Y. Chen, L. Bian, J. Liu, S. Wang, Y. Liang and Z. Liu, *Nat. Synth.*, 2022, **2**, 17.
16 J. R. Nitschke, M. Hutin and G. Bernardinelli, *Angew. Chem., Int. Ed.*, 2004, **43**, 6724.
17 X. L. Li, Z. Ma, J. Wu, Q. Zhou and J. Tang, *Dalton Trans.*, 2022, **51**, 17579.
18 M. Hutin, C. A. Schalley, G. Bernardinelli and J. R. Nitschke, *Chem. – Eur. J.*, 2006, **12**, 4069.
19 C. Browne, T. K. Ronson and J. R. Nitschke, *Angew. Chem., Int. Ed.*, 2014, **53**, 10701.
20 W. Xue, T. K. Ronson, Z. Lu and J. R. Nitschke, *J. Am. Chem. Soc.*, 2022, **144**, 6136.

21 J. P. Carpenter, T. K. Ronson, F. J. Rizzuto, T. Heliot, P. Grice and J. R. Nitschke, *J. Am. Chem. Soc.*, 2022, **144**, 8467.
22 G. Wu, Y. Chen, S. Fang, L. Tong, L. Shen, C. Ge, Y. Pan, X. Shi and H. Li, *Angew. Chem., Int. Ed.*, 2021, **60**, 16594.
23 X. C. Zhou, L. X. Wu, X. Z. Wang, Y. L. Lai, Y. Y. Ge, J. Su, X. P. Zhou and D. Li, *Inorg. Chem.*, 2022, **61**, 5196.
24 R. Lavendomme, T. K. Ronson and J. R. Nitschke, *J. Am. Chem. Soc.*, 2019, **141**, 12147.
25 R. Modak, B. Mondal, P. Howlader and P. S. Mukherjee, *Chem. Commun.*, 2019, **55**, 6711.
26 J. H. Zhang, H. P. Wang, L. Y. Zhang, S. C. Wei, Z. W. Wei, M. Pan and C. Y. Su, *Chem. Sci.*, 2020, **11**, 8885.
27 T. Hasell and A. I. Cooper, *Nat. Rev. Mater.*, 2016, **1**, 16053.
28 Y. Chen, Y. Lei, L. Tong and H. Li, *Chem. – Eur. J.*, 2022, **28**, e202102910.
29 P. S. Mukherjee and D. Chakraborty, *Chem. Commun.*, 2022, **58**, 5558.
30 J. Mosquera, S. Zarra and J. R. Nitschke, *Angew. Chem., Int. Ed.*, 2014, **53**, 1556.
31 H. Li, H. Zhang, A. D. Lammer, M. Wang, X. Li, V. M. Lynch and J. L. Sessler, *Nat. Chem.*, 2015, **7**, 1003, DOI: **10.1038/nchem.2392**.
32 F. Wang, C. Bucher, Q. He, A. Jana and J. L. Sessler, *Acc. Chem. Res.*, 2022, **55**, 1646.
33 Z. W. Li, X. Wang, L. Q. Wei, I. Ivanovic-Burmazovic and G. F. Liu, *J. Am. Chem. Soc.*, 2020, **142**, 7283.
34 F. F. Chang, F. D. Feng, J. Geng and W. Huang, *Chem. Commun.*, 2021, **57**, 9220.
35 S. L. Han, J. Yang, D. Tripathy, X. Q. Guo, S. J. Hu, X. Z. Li, L. X. Cai, L. P. Zhou and Q. F. Sun, *Inorg. Chem.*, 2020, **59**, 14023.
36 H. Yan, C. M. Wang, P. Chen, Y. Q. Zhang and W. B. Sun, *Dalton Trans.*, 2022, **51**, 6918.
37 X. Liu, X. Yang, Y. Ma, J. Liu, D. Shi and D. Schipper, *Chin. Chem. Lett.*, 2021, **32**, 569.
38 Y. Peng, H. Kaemmerer and A. Powell, *Chem. – Eur. J.*, 2021, **27**, 15044.
39 H. S. Wang, K. Zhang, Y. Song and Z. Q. Pan, *Inorg. Chim. Acta*, 2021, **521**, 120318.
40 C. L. Yin, Z. B. Hu, Q. Q. Long, H. S. Wang, J. Li, Y. Song, Z. C. Zhang, Y. Q. Zhang and Z. Q. Pan, *Dalton Trans.*, 2019, **48**, 512.
41 P. D. Frischmann, V. Kunz and F. Wurthner, *Angew. Chem., Int. Ed.*, 2015, **54**, 7285.
42 A. M. Castilla, N. Ousaka, R. A. Bilbeisi, E. Valeri, T. K. Ronson and J. R. Nitschke, *J. Am. Chem. Soc.*, 2013, **135**, 17999.
43 E. G. Percastegui, J. Mosquera, T. K. Ronson, A. J. Plajer, M. Kieffer and J. R. Nitschke, *Chem. Sci.*, 2019, **10**, 2006.
44 A. M. Castilla, T. K. Ronson and J. R. Nitschke, *J. Am. Chem. Soc.*, 2016, **138**, 2342.
45 J. Holub, A. Santoro, M.-A. Stadler and J.-M. Lehn, *Inorg. Chem. Front.*, 2021, **8**, 5054.
46 M. Urbani and T. Torres, *Chem. – Eur. J.*, 2020, **26**, 1683.
47 L. Meng, Y.-F. Deng, S. Liu, Z. Zheng and Y.-Z. Zhang, *Sci. China: Chem.*, 2021, **64**, 1340.
48 E. T. Luis, H. Iranmanesh, K. S. A. Arachchige, W. A. Donald, G. Quach, E. G. Moore and J. E. Beves, *Inorg. Chem.*, 2018, **57**, 8476.
49 Z. Wang, L. P. Zhou, T. H. Zhao, L. X. Cai, X. Q. Guo, P. F. Duan and Q. F. Sun, *Inorg. Chem.*, 2018, **57**, 7982.
50 Q. Y. Zhu, L. P. Zhou and Q. F. Sun, *Dalton Trans.*, 2019, **48**, 4479.
51 Q. Y. Zhu, L. P. Zhou, L. X. Cai, X. Z. Li, J. Zhou and Q. F. Sun, *Chem. Commun.*, 2020, **56**, 2861.
52 Q. Y. Zhu, L. P. Zhou, L. X. Cai, S. J. Hu, X. Z. Li and Q. F. Sun, *Inorg. Chem.*, 2022, **61**, 16814.
53 G. L. Zhang, L. P. Zhou, D. Q. Yuan and Q. F. Sun, *Angew. Chem., Int. Ed.*, 2015, **54**, 9844.
54 C. D. Buch, S. H. Hansen, C. M. Tram, D. Mitcov and S. Piligkos, *Inorg. Chem.*, 2020, **59**, 16328.
55 J. Wang, M. Feng, M. N. Akhtar and M.-L. Tong, *Coord. Chem. Rev.*, 2019, **387**, 129.
56 Y. Peng and A. K. Powell, *Coord. Chem. Rev.*, 2021, **426**, 213490.
57 C. B. Tian, Y. H. Han, Z. Z. He and S. W. Du, *Chem. – Eur. J.*, 2017, **23**, 767.
58 Q. Yang, G. L. Wang, Y. Q. Zhang and J. Tang, *Dalton Trans.*, 2022, **51**, 13928.
59 N. Ahmed and K. Uddin Ansari, *Dalton Trans.*, 2022, **51**, 4122.
60 E. Moreno Pineda, N. F. Chilton, F. Tuna, R. E. Winpenny and E. J. McInnes, *Inorg. Chem.*, 2015, **54**, 5930.
61 H. S. Wang, Q. Q. Long, Z. B. Hu, L. Yue, F. J. Yang, C. L. Yin, Z. Q. Pan, Y. Q. Zhang and Y. Song, *Dalton Trans.*, 2019, **48**, 13472.